Heliyon 10 (2024) e37094

Contents lists available at ScienceDirect

Heliyon

journal homepage: www.cell.com/heliyon

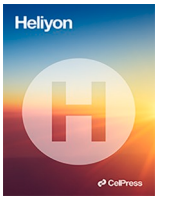

Research article

Visible and near-infrared modulating tungsten suboxide nanorods electrochromic films in acidic aqueous electrolytes

Keechul Kwon [a], Jae Hun Lee [b], Kihoon Kim [c], Sungyeon Heo [a,*]

[a] Department of Chemical and Biomolecular Engineering, Seoul National University of Science &Technology, Seoul, 01811, Republic of Korea
[b] Hydrogen Research Department, Korea Institute of Energy Research (KIER), 152 Gajeong-ro, Yuseong-gu, Daejeon, 34129, Republic of Korea
[c] Material Science Division, Argonne National Laboratory, Lemont, IL, 60439, United States

ARTICLE INFO

Keywords:
Proton insertion
Tungsten suboxide
Nanocrystals
Near-infrared modulation
Aqueous electrolytes

ABSTRACT

Proton-based aqueous electrolytes can be used to achieve high performance electrochromic nanocrystal thin films due to their small ion size. However, acidic aqueous electrolyte systems have not yet been explored in near-infrared (NIR) absorbing plasmonic tungsten oxide nanocrystal films. Here, we demonstrate tungsten suboxide nanorod films with excellent visible and NIR modulation performance in the H^+-based aqueous electrolytes, thanks to their mesoporous structure, nanosized domains, and open tunnel structure. Colloidally synthesized $WO_{2.83}$ nanorods with an average width of 6 nm and length of 48 nm were converted to $WO_{2.90}$ nanorod film via annealing in air, while still preserving open tunnels. These films exhibit fast switching speed ($t_c = 0.9$ s, $t_b = 2.1$ s), excellent cycling stability over 2500 cycles, wide optical modulation up to $\Delta T = 53.8$ % in the NIR region, and a high coloration efficiency (CE) of 167 $cm^2\ C^{-1}$ at 1300 nm. Additionally, introducing a thin spacer (25 μm) reduced intrinsic NIR absorption from water, thereby enhancing the NIR modulation properties. These highly performing aqueous proton-electrolytes-based electrochromic devices open new possibilities for implementing visible and NIR electrochromism.

1. Introduction

Escalating global energy demand and the pressing need for sustainable solutions have brought attention to the significant energy consumption associated with building cooling and heating systems. To address this issue, the development of electrochromic window technologies has gained prominence as a potential way to mitigate energy usage by controlling the transmission of sunlight into buildings [1,2]. Conventional materials managing visible light transmittance through polaronic absorption endow individual privacy and glare control [3–6]. Near-infrared (NIR) modulation from plasmonic doped metal oxide nanocrystal thin films, first introduced by Milliron group, has demonstrated a promising solution for efficient thermal control, enabling visible and NIR dual-band modulation [7–12].

Among doped metal oxide nanocrystals, colloidal tungsten suboxide is one of the strong candidates for electrochromic application due to its excellent absorption properties in both visible and NIR ranges [13,14]. The crystal structure and shape of tungsten oxide nanocrystals can be adjusted based on the oxygen vacancy concentrations and growth conditions [15–17]. The variation in ion insertion sites along different crystallographic directions becomes evident when comparing different crystal shapes. Heo et al.

* Corresponding author.
E-mail address: sungyeonh@seoultech.ac.kr (S. Heo).

https://doi.org/10.1016/j.heliyon.2024.e37094
Received 7 August 2024; Accepted 22 August 2024
Available online 30 August 2024

examined the influence of hexagonal tungsten oxide nanocrystals' crystalline and shape anisotropy on the optical modulation with varying sizes of Li^+, Na^+, TBA^+ ions [18]. This study indicates that selecting electrolytes with appropriate ion sizes can enhance coloration efficiency (CE) and charge capacity.

Compared to other electrolyte cations, proton (H^+) electrolytes, which have the highest diffusion coefficient and small ionic radius, offer advantages in insertion chemistry, leading to faster response times and larger capacities [19,20]. However, using proton electrolytes in WO_3 is largely limited by poor chemical stability in acidic environments. Hu et al. revealed that the electrochemical degradation of WO_3 thin films with acidic electrolytes primarily stems from the irreversible proton trapping during the intercalation and deintercalation processes, as well as tungsten dissolution/redeposition [21]. They also noted that degradation is exacerbated when the charge heterogeneity developes, particularly in larger domain sizes. Consequently, unlike introducing other conventional ions, introducing protons has a trade-off between its stability issues and fast response with high performance. These fatal flaws hinder the advancement of proton-electrolyte-based electrochromic devices with long-term stability.

Despite the advantages of H^+-based electrolytes, their use in visible and NIR modulating tungsten oxide nanocrystal thin films has been scarcely reported. Since H^+ diffusion length and insertion kinetics are strongly influenced by the size of host materials and the crystal structure, colloidal tungsten oxide nanocrystals are promising for the following reasons. First, colloidally synthesized tungsten oxide nanocrystals have intrinsic oxygen vacancies in the crystal structure, which induce open tunnel sites that facilitate easy proton insertion. Second, the oxygen vacancies also increase the electron concentration, enhancing electronic properties and enabling fast electrochemical switching. It has been reported that oxygen-deficient tungsten suboxide (WO_{3-x}) shows improved conductivity and electron transport in supercapacitor applications [22]. Third, the nanoscale size of tungsten oxide reduces the ion diffusion path length, mitigating the ion trapping event which is advantageous for acidic electrolytes system. Lastly, the plasmonic properties of these nanocrystals allow for efficient absorption of the NIR light [23]. We hypothesized that these synergetic properties of tungsten suboxide nanocrystals could improve electrochromic performance even in the acidic electrolytes system.

Herein, we present highly performed electrochromic tungsten oxide nanocrystal thin films in 0.5 M H_2SO_4 electrolytes. The colloidally synthesized $WO_{2.83}$ nanorods have an average width of 6 nm and a length of 48 nm. These nanorods exhibit localized surface plasmon resonance (LSPR) absorption properties in the visible and NIR range due to free electrons generated from oxygen vacancies and their small size. Spin-coated films annealed in air still preserves oxygen vacancies with open tunnels. These properties result in strong modulation properties with a high CE of 167 cm^2/C at 1300 nm, fast switching speed ($t_c = 0.9$ s, $t_b = 2.1$ s), and good stability over 2500 cycles. Furthermore, we found that reducing the spacing between the counter and working electrodes enhances modulation in the NIR range, highlighting the trade-off between NIR modulation and water absorption properties. Our research demonstrates the significant potential of tungsten suboxide nanocrystals for proton-based electrolyte electrochromic applications.

2. Experimental

2.1. Synthesis of $WO_{2.83}$ nanorods

The synthesis of $WO_{2.83}$ nanorods was carried out with standard Schlenk line techniques by adapting a procedure reported by Manthiram et al. [24]. 11.1875 g of oleic acid (Sigma Aldrich, 90 %) and 14.175 g of trioctylamine (Sigma Aldrich, 98 %) were mixed in a 100 ml three-neck flask and degassed under vacuum at 120 °C for 1 h. The flask was then placed under N_2 atmosphere and heated to 310 °C. 0.5 ml of tungsten (V) ethoxide (Thermo Scientific, 95 %) was rapidly injected and the reaction was held at 310 °C for 5 min. After the reaction finished, the reacted mixture was cooled to room temperature, and the solution was precipitated. The acetone washing step was repeated twice, and the nanorods were resuspended in acetone at a concentration of 50 mg/ml.

2.2. Fabrication of $WO_{2.90}$ nanorods thin film

Before deposition of the nanorod solution, 2.5 cm × 3 cm FTO substrates were prepared by following steps. First, substrates were sonicated with acetone for 30 min, then cleaned again with isopropyl alcohol for 30 min. For the coating of tungsten suboxide nanorods, substrates were additionally sonicated in acetone for 30 min. As-synthesized ligand-capped $WO_{2.83}$ nanorods dispersed in acetone (50 mg/mL) were spin-coated at 1500 rpm for 2 min. The deposited thin films were annealed at 400 °C for 30 min to remove the organic ligands on the nanocrystal surface and confirmed to be in the $WO_{2.90}$ crystal phase by the XRD measurement.

2.3. Preparation and assembly of the electrochromic device

Sandwich-type electrochromic devices were fabricated with a working electrode ($WO_{2.90}$ nanocrystal film) and a Pt counter electrode with varied spacing (25 μ m and 180 μ m). Pt-coated counter electrodes were prepared via spin coating a 7 mM H_2PtCl_6 solution in isopropyl alcohol onto FTO glass substrates followed by calcination in air at 450 °C for 30 min.

2.4. Sample characterization

The surface morphology of the nanocrystal thin films on the silicon wafer was characterized using scanning electron microscopy (SEM, TESCAN VEGA3). TEM images were obtained with a JEM 2100F, JEOL. Solutions for TEM measurement were prepared by drop-casting on the copper TEM grids with carbon support films. The crystal structures of thin films were determined using X-ray diffractometer (XRD, Bruker DE/D8 Advance) at a scan speed of 1 °/min, ranging between 2 θ = 10° and 50°. X-ray Photoelectron

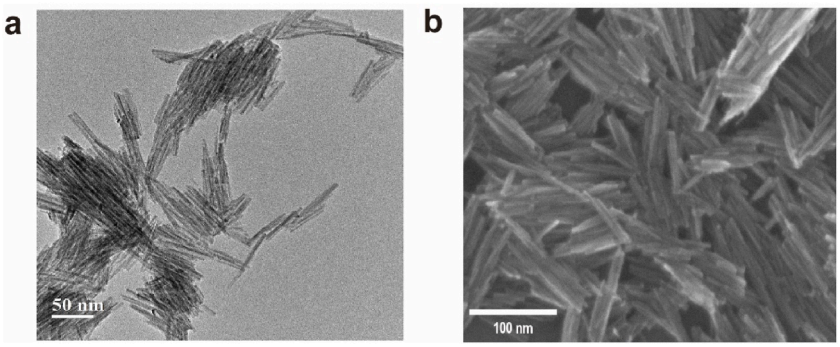

Fig. 1. Structural properties of the as-synthesized $WO_{2.83}$ nanorods. (a) TEM and (b) SEM images of the $WO_{2.83}$ nanorods.

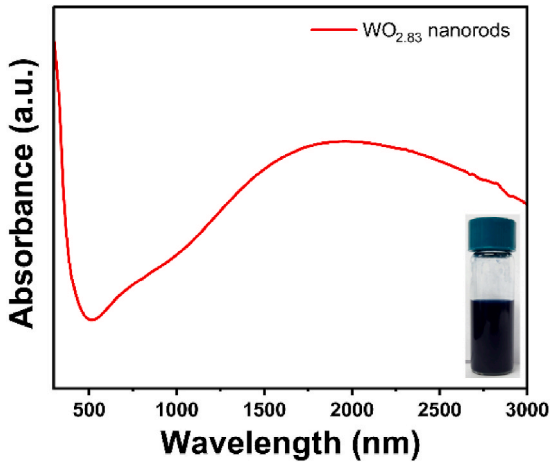

Fig. 2. UV-Vis-NIR absorption spectra of the as-synthesized $WO_{2.83}$ nanorods solution dispersed in tetrachloroethylene. (Inset: an optical photo of the dispersed nanocrystal solution which appears pale blue).

Spectrometer (XPS) measurement were acquired on a Thermo Fisher Scientific Brno s.r.o (Nexsa).

2.5. In situ spectroelectrochemical measurement

A home built in situ spectroelectrochemical cell was used to characterize the electrochromic properties of the deposited thin films. $WO_{2.90}$ nanorods coated on FTO glass as the working electrode were immersed in the 0.5 M H_2SO_4 electrolytes in a three-electrode system (the cell was illuminated with a light source). Pt wire was used as the counter electrode and Ag/AgCl was used as the reference electrode. Potentiostat (Biologic, SP-300) was used for chronoamperometry (CA) and cyclic voltammetry (CV) studies. Optical transmission spectra (300 nm–1600 nm) were collected in situ with Oceanview 2.0 software.

3. Results and discussion

3.1. Morphology, structure, and composition of tungsten suboxide nanorods film

To increase the surface area for capacitive charging and shorten the proton diffusion length which can decrease the proton trapping with successive degradation, we synthesized $WO_{2.83}$ nanorods through the hot injection of tungsten (V) ethoxide into a solvent mixture of oleic acid and trioctylamine under an N_2 atmosphere (See the experimental section). Transmission electron microscopy (TEM) measurement revealed that the nanorods have an average width of 6 nm and an average length of 48 nm (Fig. 1a). This short proton path length is expected to enhance ion insertion kinetics and reduce the proton trapping, thereby improving cycling stability.

The inherent oxygen vacancies support high free electron concentration with localized surface plasmon resonance properties (LSPR). The rod-like morphology is also well revealed by UV-Vis-NIR absorption spectra measurements. The transverse and longitudinal polarization modes contribute to the strong LSPR absorption features in the visible and NIR range (Fig. 2). Fig. 2 shows a distinct peak centered at 1800 nm, indicating that $WO_{2.83}$ nanorods exhibit strong LSPR absorption across the entire NIR region, overlapping well with the solar spectrum.

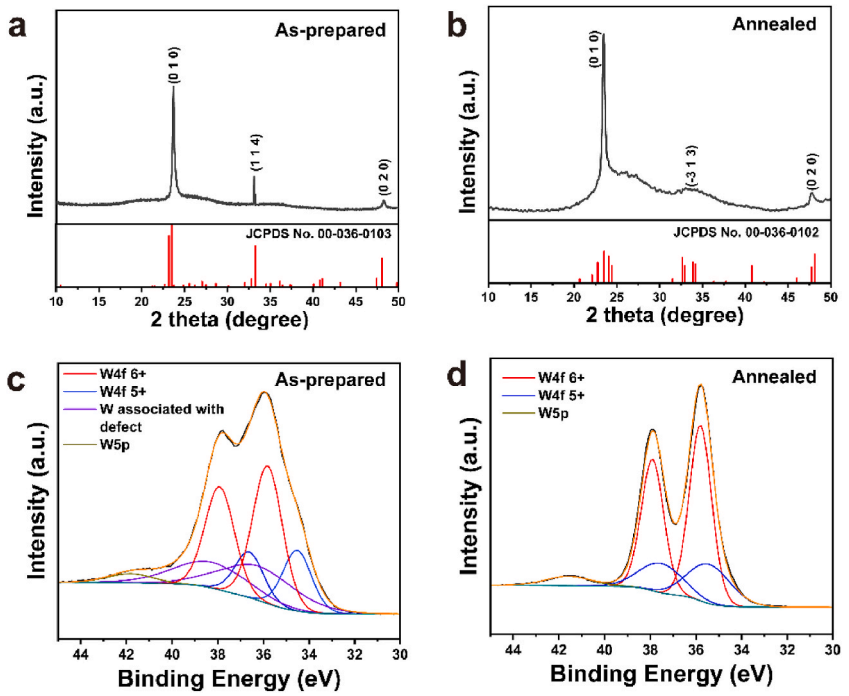

Fig. 3. X-ray diffraction (XRD) patterns of the tungsten oxide nanorods film before (a), and after thermal treatment (b) and X-ray photoelectron spectroscopy (XPS) spectra of the tungsten oxide nanorods film before (c) and after thermal treatment (d).

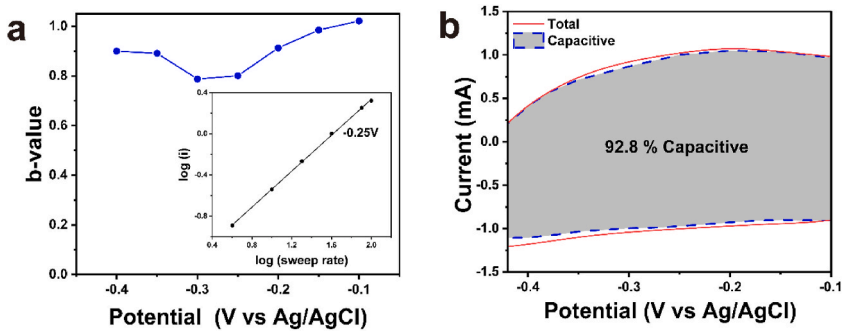

Fig. 4. (a) b-values for the $WO_{2.90}$ nanorods film plotted as a function of potential during cathodic sweeps (H^+ insertion), Inset: power law dependence of current on sweep rate at −0.25 V (vs Ag/AgCl), (b) Voltammetric response at a sweep rate of 40 mV/s for $WO_{2.90}$ nanorods films, with the capacitive contribution shaded.

The synthesized tungsten suboxide nanocrystals contain oxygen vacancies that create open tunnels, such as trigonal and square tunnels, depending on the extent of these vacancies [25]. The X-ray diffraction (XRD) patterns of the tungsten oxide film are shown in Fig. 3a. The XRD pattern of the as-prepared tungsten oxide film reveals that the nanocrystals exhibit a monoclinic $WO_{2.83}$ structure (JCPDS No 00-036-0103). The spin-coated nanorod film exhibits a randomly packed arrangement, resulting in a porous thin film morphology. This porous nature is expected to facilitate easy ion diffusion into the nanocrystal thin films, as demonstrated in the previous study [26].

To remove the insulating layer originating from ligands, thermal treatment was processed under oxidizing conditions. The distinct peaks in the XRD results in Fig. 3b correspond well with (010), (−313), and (020) diffractions with good agreements of $WO_{2.90}$ crystal phase (JCPDS No 00-036-0102). X-ray photoelectron spectroscopy (XPS) revealed that two states of W atoms (W^{5+} and W^{6+}) coexist in both the as-prepared and annealed film. (Fig. 3c and d). Following thermal annealing, oxygen incorporation was inevitable, so that the fraction of W^{6+} increased from 49 % to 70 % as shown in the XPS data (Fig. 3c and d). Despite the thermal annealing, oxygen vacancies were preserved, evidenced by the presence of W^{5+}, and reflected in the XRD crystal phase. The presence of reduced W^{5+} states is expected to enhance efficient charge injection due to the abundant electron concentration [27].

One of the dominant coloration mechanisms involves charge transfer between two different valence states of W atoms [4,28]. Therefore, a larger fraction of W^{6+} is necessary for greater modulation. The increase in the W^{6+} fraction after the annealing process

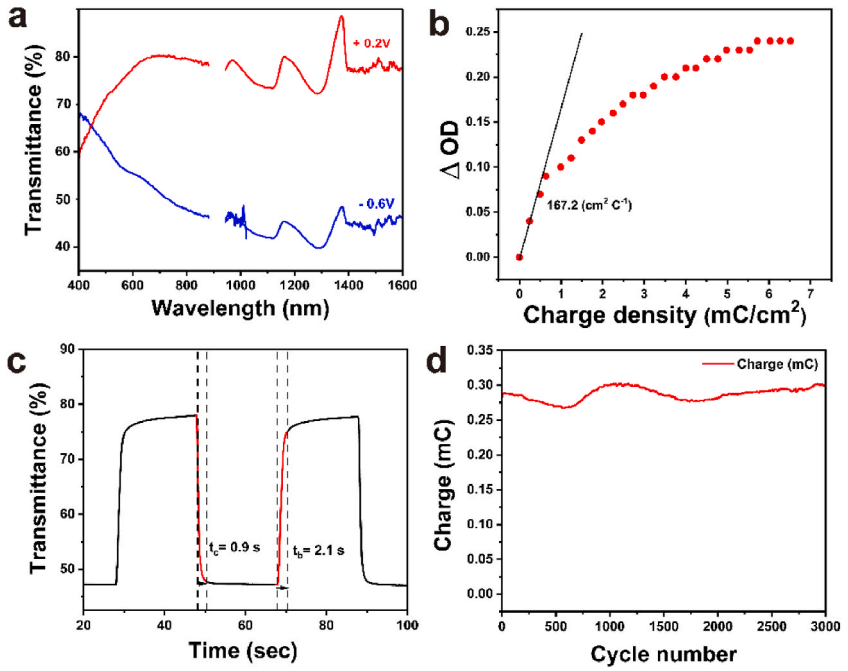

Fig. 5. Electrochromic characteristics of $WO_{2.90}$ nanorods in 0.5 M H_2SO_4 (aq) electrolytes: (a) UV–Vis transmittance curves measured at +0.2 V (bleached state) and −0.6 V (colored state). The discontinuous spectral band, due to the different visible and NIR spectrometers, is shown as a blank region. (b) Plot of optical density (OD) change with respect to the charge density measured at a 1 C rate. (c) The response time tested by alternately applying −0.6 V and +0.2 V (vs. Ag/AgCl). (d) Cycling stability shown as charge to the cycle number.

underscores the significance of annealing, not only for removing the insulating ligands but also for enhancing electrochromic properties.

3.2. *Analysis of the charging mechanism of $WO_{2.90}$ nanorods film (half cell)*

Cyclic voltammetry (CV) was conducted within the potential range of −0.5 to 0.5 V (vs Ag/AgCl) in a three-electrode cell to investigate the electrochemical performance of the thin film. Fig. S1 presents the CV curve of $WO_{2.90}$ nanorods thin film, which is in accordance with typical CV curves of nanocrystalline tungsten oxide films reported previously [29,30]. The curves exhibit reversible behavior within the potential range, indicating that the introduction of protons into the tungsten suboxide results in excellent electrochemical insertion properties.

CV curves at various scanning rates ranging from 4 to 200 mV/s were analyzed to examine the proton insertion kinetics (Fig. S2). It is well known that electrochemical charging behavior arises from two different mechanisms: the capacitive-like process and the diffusion-controlled process [31]. The currents change in the inset of Fig. 4a follow the following equation:

$$i = av^b$$

where i represents the current, v is the scan rate, and a and b are adjustable parameters. When the b value is 0.5, the current is controlled by semi-infinite diffusion. On the other hand, when b value is close to 1, the current is proportional to the sweep rate, meaning that the capacitive charging is the dominant mechanism. As shown in Fig. 4a, the b values obtained at various potentials ranging from −0.1 V to −0.4 V are close to 1, indicating that the current primarily arises from the capacitive behavior [32].

The dominance of the capacitive charge mechanism can also be inferred from CV tests conducted at various scan rates using different methods (Figs. S2 and S3). The current response at a fixed potential can be expressed as a combination of two mechanisms: the diffusion-controlled insertion process and the capacitive process, described by the following equation:

$$i(V) = k_1 v\ (capacitive) + k_2 v^{\frac{1}{2}}\ (diffusion - controlled)$$

in which $k_1 v$ represents the current contributions from the capacitive-like process, and $k_2 v^{1/2}$ corresponds to the current from diffusion-controlled insertion process. Determining k_1 by fitting the current at different scan rates (Fig. 4b) revealed that capacitive charge contribution accounted for 92 % of the total. This dominant capacitive charging behavior indicates that fast electrochemical charging and discharging can be expected.

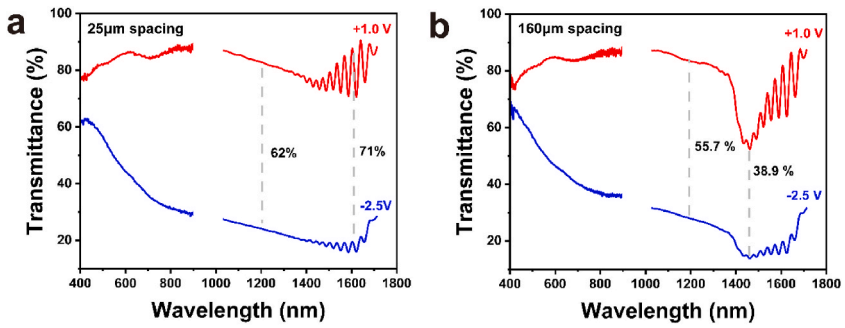

Fig. 6. (a) Vis-NIR transmittance curves of electrochromic devices with 25 μm spacing measured at 1 V (bleached state) and −2.5 V (colored state), respectively. (b) Vis-NIR transmittance spectra of electrochromic devices with 180 μm spacing measured at 1 V (bleached state) and −2.5 V (colored state), respectively. The discontinuous spectral band, due to the different visible and NIR spectrometers, is shown as a blank region.

3.3. Electrochromic properties of $WO_{2.90}$ nanorods film (half-cell)

To further confirm the electrochromic properties of $WO_{2.90}$ nanorod films, spectroelectrochemical measurements were conducted using an in situ spectro-electrochemical cell in a three-electrode configuration (See experimental section). In general, four typical parameters determine the performance of electrochromic materials: cycling stability, CE, optical modulation, and response time, all of which are closely interrelated.

Fig. 5a shows the in-situ UV–Vis transmission spectra of the $WO_{2.90}$ nanorods film tested by applying +0.2 V for bleached states and −0.6 V (vs Ag/AgCl) for colored states under moderate conditions (See Fig. S4 in Supporting Information). The difference in transmittance between the colored and bleached states demonstrates that our film turns deep blue during the charging process and exhibits good coloration and switching characteristics, particularly in the NIR region. This indicates the promising potential of our film for application in NIR-blocking energy-saving smart windows.

CE, as another important parameter of electrochromic material, was calculated using following equations,

$$\Delta OD(\lambda) = \log(T_b / T_c)$$

$$\mathrm{CE}\ (\lambda) = \Delta \mathrm{OD}/\mathrm{Q}$$

where ΔOD is the change in optical density (OD) measured at wavelength (λ), T_b and T_c denote the transmittance of the tungsten oxide film in their bleached and colored states, respectively, and Q is the charge density (C cm^{-2}). As shown in Fig. 5b, our $WO_{2.90}$ nanorods film achieved a high CE of the value 167 cm^2/C at λ = 1300 nm, surpassing the performance of other proton insertion electrochromic systems based on tungsten oxide [33–35]. This high CE indicates that our system operates with low energy consumption during the coloring process, providing significant optical modulation with minimal charge insertion/extraction. Furthermore, the superior CE achieved holds the potential to improve long-term cycling stability by addressing the persistent issue of instability in existing electrochromic systems that rely on proton electrolytes.

The response time, defined as the time required for 90 % of optical change during the coloring or bleaching process, was determined using the chronoamperometric method with −0.6 V (coloring states) and +0.2 V (bleached states) applied. Fig. 5c shows the in-situ transmittance curves at 1300 nm. Rapid switching was achieved with $t_c = 0.9$ s for coloring and $t_b = 2.1$ s for bleaching at 1300 nm. This fast switching kinetic is well explained by a substantial capacitive charge portion, as indicated in Fig. 4. We demonstrated that the introduction of a nanorod morphology with a short diffusion length, coupled with proton intercalation/deintercalation, exhibits synergistic effects that significantly shorten the response time.

Lastly, the cycling stability shown by the charge retention within 3000 cycles (Fig. 5d) confirms stable charge retention, which correlates well with the CE results shown in Fig. 5b. Fig. S5 presents a top-view SEM image of our film after 1000 cycles of charge and discharge process. The top view image of our film after cycling process shows well-maintained nanorod features, offering visual evidence of its good cycling stability. This observation closely corresponds with a previous study conducted by Rui et al., which compared the long-term cycling stability of WO_3 and WO_{3-x} electrodes [22]. WO_{3-x} exhibited well-maintained nanorod structures, while WO_3 electrodes suffered severe damage, including aggregation and degradation, after cycling. These findings suggest that oxygen vacancies contribute to enhanced cycling stability, facilitating reversible redox reactions and accommodating structural strain.

In general, achieving high electrochromic performance, including wide optical modulation, usually involves trade-off with stability issues. This challenge is particularly pronounced in previous approaches that utilize acidic aqueous electrolytes such as H_2SO_4 (aq). However, our system collaborating with randomly packed mesoporous $WO_{2.90}$ nanorods with proton intercalation/deintercalation successfully alleviates these issues and offers great potential for smart window applications.

The measurements of four crucial parameters affirm the excellent potential of our designed system for applications in electrochromic devices. The electrochemical features of our film can be attributed to the combination of nanocrystalline characteristics and proton insertion introduced into tungsten suboxide matrix. The nanocrystalline construction offers a regular lattice arrangement, which provides a large active surface area, ease of ionic diffusion, and short-range diffusion path length.

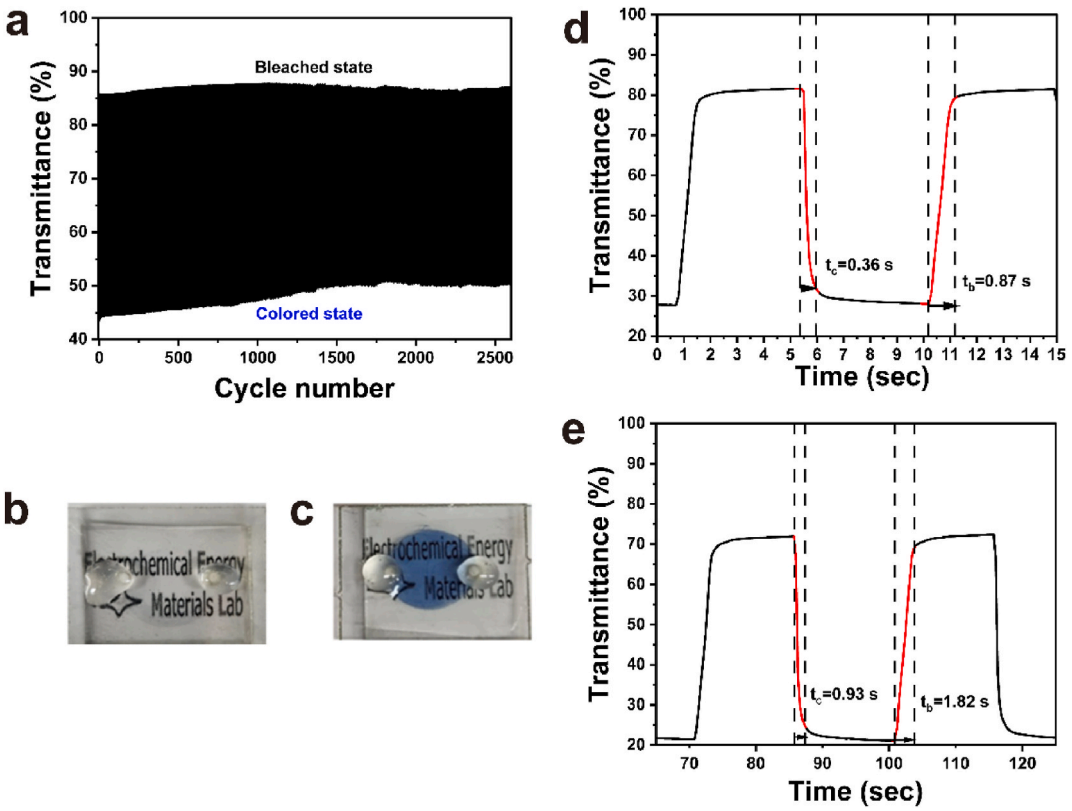

Fig. 7. (a) In-situ transmittance curves of electrochromic devices with 25 μm spacing in bleached and colored states recorded at different voltages from 1 V to −2.5 V (vs Ag/AgCl) (b, c) Optical photos of the electrochromic devices in bleached state (b) and colored state (c). (d) The response time tested by alternately applying −2.5 V (vs. Ag/AgCl) and +1.0 V (vs. Ag/AgCl) to devices in (d) initial condition and (e) after 1000 cycles.

3.4. Electrochromic properties of full cell devices

To investigate the practical utilization of $WO_{2.90}$ nanorods thin films in electrochromic devices, we designed electrochromic devices using $WO_{2.90}$/FTO electrode film as the working electrode, Pt-coated FTO glass as the counter electrode, and 0.5 M H_2SO_4 (aq) as the electrolytes. These devices were assembled in sandwich-like configurations (refer to the schematic image of electrochromic devices on Scheme S1 in the Supporting Information). One challenge associated with aqueous electrolytes in electrochromic devices is their inherent NIR absorption due to water molecules. As shown in Fig. S6, the significant NIR light absorption from water in electrolytes poses a potential challenge to maximizing optical modulation range between colored and bleached modes in electrochromic devices. Thus, we investigated the effect of spacing thickness on the electrochromic NIR modulation. Fig. 6a shows the optical transmittance spectra of electrochromic devices with a spacing of 25 μm. For electrochromic modulation, +1.0 V and −2.5 V (vs Ag/AgCl) were applied for each bleached and colored state, with the potential range determined to optimize energy efficiency while achieving a wide optical modulation range (Fig. S7). Compared to Fig. 6b (device constructed with a 180 μm thickness of aqueous electrolyte layer), the reduced spacing provides greater electrochromic modulation between the two different modes. Fig. 6a demonstrates that our electrochromic devices with 25 μm spacing achieved ΔT = 62–71 % across the visible to NIR region.

We investigated the long-term device stability. Fig. 7a shows the in-situ transmittance obtained by chronoamperometric test under condition of applying −2.5 V (colored states) and +1.0 V (bleached states), operated for 2500 cycles (total 18000 s). The device exhibits excellent retention of transmittance in the bleaching mode (86 %) and symmetrical characteristics. The transmittance was modulated from 45 % to 86 % initially, although ~10 % decrease in transmittance contrast was observed over the cycles, good stability maintenance was evident. Given the rapid electrochemical degradation of tungsten oxide nanocrystal thin films without surface treatment using nonaqueous electrolytes [36,37], the stability achieved in this system demonstrates that the proton-based aqueous system is promising for developing stable NIR-modulating electrochromic devices. Digital photos of electrochromic devices with 25 μm spacing in their bleached and colored states are presented in Fig. 7b and c, respectively, showing a tinted blue color in the colored states.

Lastly, the response time between the colored and bleached states was evaluated at 1300 nm. Fig. 7d, which was tested in its initial condition, demonstrates very fast switching speed (t_b = 0.87 s, and t_c = 0.36 s), well explained by capacitive charging induced by introducing protons. The fast-switching kinetics were slightly decreased as the cycling progressed. Fig. 7e reveals that the devices tested after 1000 cycles required an additional 25.8 % of the time to achieve 90 % of their fully charged (colored) states (t_b = 1.82 s,

and t_c = 0.93 s). The declining switching speeds observed during the cycling process, especially in the coloring process, may be attributed to the dissolution/redeposition of tungsten suboxide and ion trapping, as previously reported [22].

4. Conclusions

In summary, we demonstrated high-performance electrochromic devices using aqueous acidic electrolytes and tungsten suboxide nanocrystals capable of modulating visible and NIR light. The fabricated full cell electrochromic devices exhibit rapid switching within 1 s, high CE of 167 cm^2/C at 1300 nm, and excellent cycling stability over 2500 cycles. The visible and NIR electrochromic properties arise from the LSPR absorption of tungsten suboxides. The short diffusion length and open tunnels of the nanorods, combined with the random morphology of the thin films, facilitate proton insertion. Introducing a thin spacing layer in the device reduces NIR absorption from water, highlighting the importance of device design. Our results indicate that proton-based electrolyte systems hold promise for developing next-generation electrochromic thin films using colloidal doped tungsten suboxide nanocrystals.

Data availability

Data will be available upon request.

CRediT authorship contribution statement

Keechul Kwon: Data curation, Investigation, Writing – original draft. **Jae Hun Lee:** Writing – review & editing. **Kihoon Kim:** Writing – review & editing. **Sungyeon Heo:** Conceptualization, Funding acquisition, Investigation, Supervision, Writing – original draft.

Declaration of competing interest

The authors declare that they have no known competing financial interests or personal relationships that could have appeared to influence the work reported in this paper.

Acknowledgment

This study was supported by the Research Program funded by the SeoulTech(Seoul National University of Science and Technology).

Appendix A. Supplementary data

Supplementary data to this article can be found online at https://doi.org/10.1016/j.heliyon.2024.e37094.

References

[1] J. Wang, E. Khoo, P.S. Lee, J. Ma, Synthesis, assembly, and electrochromic properties of uniform crystalline WO_3 nanorods, J. Phys. Chem. C 112 (2008) 14306–14312, https://doi.org/10.1021/jp804035r.
[2] D. Ma, T. Li, Z. Xu, L. Wang, J. Wang, Electrochromic devices based on tungsten oxide films with honeycomb-like nanostructures and nanoribbons array, Sol. Energy Mater. Sol. Cells 177 (2018) 51–56, https://doi.org/10.1016/j.solmat.2017.06.009.
[3] J. Guo, X. Guo, H. Sun, Y. Xie, X. Diao, M. Wang, X. Zeng, Z.-B. Zhang, Unprecedented electrochromic stability of a-WO_{3-x} thin films achieved by using a hybrid-cationic electrolyte, ACS Appl. Mater. Interfaces 13 (2021) 11067–11077, https://doi.org/10.1021/acsami.0c22921.
[4] C.G. Granqvist, Electrochromics for smart windows: oxide-based thin films and devices, Thin Solid Films 564 (2014) 1–38, https://doi.org/10.1016/j.tsf.2014.02.002.
[5] S. Adhikari, D. Sarkar, Hydrothermal synthesis and electrochromism of WO_3 nanocuboids, RSC Adv. 4 (2014) 20145, https://doi.org/10.1039/c4ra00023d.
[6] D. Ma, H. Niu, J. Huang, Q. Li, J. Sun, H. Cai, Z. Zhou, J. Wang, Porous $NiMoO_4$ nanosheet films and a device with ultralarge optical modulation for electrochromic energy-storage applications, Nano Lett. 24 (2024) 814–821, https://doi.org/10.1021/acs.nanolett.3c03270.
[7] E.L. Runnerstrom, A. Llordés, S.D. Lounis, D.J. Milliron, Nanostructured electrochromic smart windows: traditional materials and NIR-selective plasmonic nanocrystals, Chem. Commun. 50 (2014) 10555, https://doi.org/10.1039/C4CC03109A.
[8] A. Llordés, G. Garcia, J. Gazquez, D.J. Milliron, Tunable near-infrared and visible-light transmittance in nanocrystal-in-glass composites, Nature 500 (2013) 323–326, https://doi.org/10.1038/nature12398.
[9] S. Heo, J. Kim, G.K. Ong, D.J. Milliron, Template-free mesoporous electrochromic films on flexible substrates from tungsten oxide nanorods, Nano Lett. 17 (2017) 5756–5761, https://doi.org/10.1021/acs.nanolett.7b02730.
[10] T. Bai, W. Li, G. Fu, Q. Zhang, K. Zhou, H. Wang, Dual-band electrochromic smart windows towards building energy conservation, Sol. Energy Mater. Sol. Cells 256 (2023) 112320, https://doi.org/10.1016/j.solmat.2023.112320.
[11] S. Cao, S. Zhang, T. Zhang, Q. Yao, J.Y. Lee, A visible light-near-infrared dual-band smart window with internal energy storage, Joule 3 (2019) 1152–1162, https://doi.org/10.1016/j.joule.2018.12.010.
[12] S. Park, H.S. Park, T.T. Dao, S.H. Song, S.I. Lee, H.V. Tran, A. Ullah, C.-H. Han, S. Hong, Solvothermal synthesis of oxygen deficient tungsten oxide nano-particle for dual band electrochromic devices, Sol. Energy Mater. Sol. Cells 242 (2022) 111759, https://doi.org/10.1016/j.solmat.2022.111759.
[13] R. Giannuzzi, R. Scarfiello, T. Sibillano, C. Nobile, V. Grillo, C. Giannini, P.D. Cozzoli, M. Manca, From capacitance-controlled to diffusion-controlled electrochromism in one-dimensional shape-tailored tungsten oxide nanocrystals, Nano Energy 41 (2017) 634–645, https://doi.org/10.1016/j.nanoen.2017.09.058.

[14] S. Zeb, G. Sun, Y. Nie, H. Xu, Y. Cui, X. Jiang, Advanced developments in nonstoichiometric tungsten oxides for electrochromic applications, Mater. Adv. 2 (2021) 6839–6884, https://doi.org/10.1039/D1MA00418B.
[15] Y. Cheref, F. Lochon, L. Daugas, C. Cleret De Langavant, É. Larquet, A. Baron, T. Gacoin, J. Kim, Dual-band LSPR of tungsten bronze nanocrystals tunable over NIR and SWIR ranges, Chem. Mater. 34 (2022) 9795–9802, https://doi.org/10.1021/acs.chemmater.2c02879.
[16] S. Zhang, S. Cao, T. Zhang, Q. Yao, A. Fisher, J.Y. Lee, Monoclinic oxygen-deficient tungsten oxide nanowires for dynamic and independent control of near-infrared and visible light transmittance, Mater. Horiz. 5 (2018) 291–297, https://doi.org/10.1039/C7MH01128H.
[17] S. Cong, F. Geng, Z. Zhao, Tungsten oxide materials for optoelectronic applications, Adv. Mater. 28 (2016) 10518–10528, https://doi.org/10.1002/adma.201601109.
[18] S. Heo, S.H. Cho, C.J. Dahlman, A. Agrawal, D.J. Milliron, Influence of crystalline and shape anisotropy on electrochromic modulation in doped semiconductor nanocrystals, ACS Energy Lett. 5 (2020) 2662–2670, https://doi.org/10.1021/acsenergylett.0c01236.
[19] Z. Shao, A. Huang, C. Ming, J. Bell, P. Yu, Y.-Y. Sun, L. Jin, L. Ma, H. Luo, P. Jin, X. Cao, All-solid-state proton-based tandem structures for fast-switching electrochromic devices, Nat. Electron. 5 (2022) 45–52, https://doi.org/10.1038/s41928-021-00697-4.
[20] S.-H. Lee, R. Deshpande, P.A. Parilla, K.M. Jones, B. To, A.H. Mahan, A.C. Dillon, Crystalline WO_3 nanoparticles for highly improved electrochromic applications, Adv. Mater. 18 (2006) 763–766, https://doi.org/10.1002/adma.200501953.
[21] A. Hu, Z. Jiang, C. Kuai, S. McGuigan, D. Nordlund, Y. Liu, F. Lin, Uncovering phase transformation, morphological evolution, and nanoscale color heterogeneity in tungsten oxide electrochromic materials, J. Mater. Chem. A 8 (2020) 20000–20010, https://doi.org/10.1039/D0TA06612E.
[22] R. Wang, Y. Lu, L. Zhou, Y. Han, J. Ye, W. Xu, X. Lu, Oxygen-deficient tungsten oxide nanorods with high crystallinity: promising stable anode for asymmetric supercapacitors, Electrochim. Acta 283 (2018) 639–645, https://doi.org/10.1016/j.electacta.2018.06.188.
[23] G. Li, S. Zhang, C. Guo, S. Liu, Absorption and electrochromic modulation of near-infrared light: realized by tungsten suboxide, Nanoscale 8 (2016) 9861–9868, https://doi.org/10.1039/C5NR09147K.
[24] K. Manthiram, A.P. Alivisatos, Tunable localized surface plasmon resonances in tungsten oxide nanocrystals, J. Am. Chem. Soc. 134 (2012) 3995–3998, https://doi.org/10.1021/ja211363w.
[25] A. Polaczek, M. Pekala, Z. Obuszko, Magnetic susceptibility and thermoelectric power of tungsten intermediary oxides, J. Phys. Condens. Matter 6 (1994) 7909, https://doi.org/10.1088/0953-8984/6/39/011.
[26] G. Cai, M. Cui, V. Kumar, P. Darmawan, J. Wang, X. Wang, A. Lee-Sie Eh, K. Qian, P.S. Lee, Ultra-large optical modulation of electrochromic porous WO_3 film and the local monitoring of redox activity, Chem. Sci. 7 (2016) 1373–1382, https://doi.org/10.1039/C5SC03727A.
[27] C. Huez, M. Berthe, F. Volatron, J.-M. Guigner, D. Brouri, L.-M. Chamoreau, B. Baptiste, A. Proust, D. Vuillaume, Highly conductive tungsten suboxide nanotubes, J. Appl. Phys. 134 (2023) 134301, https://doi.org/10.1063/5.0170761.
[28] S.K. Deb, Opportunities and challenges in science and technology of WO_3 for electrochromic and related applications, Sol. Energy Mater. Sol. Cells 92 (2008) 245–258, https://doi.org/10.1016/j.solmat.2007.01.026.
[29] E. Ozkan, Electrochromic and optical properties of mesoporous tungsten oxide films, Solid State Ion 149 (2002) 139–146, https://doi.org/10.1016/S0167-2738(02)00143-1.
[30] D. Zhou, B. Che, J. Kong, X. Lu, A nanocrystalline tungsten oxide electrochromic coating with excellent cycling stability prepared via a complexation-assisted sol–gel method, J. Mater. Chem. C 4 (2016) 8041–8051, https://doi.org/10.1039/C6TC03194C.
[31] T. Brezesinski, J. Wang, S.H. Tolbert, B. Dunn, Ordered mesoporous α-MoO_3 with iso-oriented nanocrystalline walls for thin-film pseudocapacitors, Nat. Mater. 9 (2010) 146–151, https://doi.org/10.1038/nmat2612.
[32] P. Yang, P. Sun, L. Du, Z. Liang, W. Xie, X. Cai, L. Huang, S. Tan, W. Mai, Quantitative analysis of charge storage process of tungsten oxide that combines pseudocapacitive and electrochromic properties, J. Phys. Chem. C 119 (2015) 16483–16489, https://doi.org/10.1021/acs.jpcc.5b04707.
[33] J. De Ribamar Martins Neto, R.M. Torresi, S. I, Cordoba De Torresi, Electrochromic behavior of WO_3 nanoplate thin films in acid aqueous solution and a protic ionic liquid, J. Electroanal. Chem. 765 (2016) 111–117, https://doi.org/10.1016/j.jelechem.2015.08.032.
[34] J. Wang, E. Khoo, P.S. Lee, J. Ma, Controlled synthesis of WO_3 nanorods and their electrochromic properties in H_2SO_4 electrolyte, J. Phys. Chem. C 113 (2009) 9655–9658, https://doi.org/10.1021/jp901650v.
[35] C.Y. Ng, K. Abdul Razak, Z. Lockman, Effect of annealing on acid-treated $WO_3{\cdot}H_2O$ nanoplates and their electrochromic properties, Electrochim. Acta 178 (2015) 673–681, https://doi.org/10.1016/j.electacta.2015.08.069.
[36] S. Heo, C.J. Dahlman, C.M. Staller, T. Jiang, A. Dolocan, B.A. Korgel, D.J. Milliron, Enhanced coloration efficiency of electrochromic tungsten oxide nanorods by site selective occupation of sodium ions, Nano Lett. 20 (2020) 2072–2079, https://doi.org/10.1021/acs.nanolett.0c00052.
[37] J. Kim, G.K. Ong, Y. Wang, G. LeBlanc, T.E. Williams, T.M. Mattox, B.A. Helms, D.J. Milliron, Nanocomposite architecture for rapid, spectrally-selective electrochromic modulation of solar transmittance, Nano Lett. 15 (2015) 5574–5579, https://doi.org/10.1021/acs.nanolett.5b02197.